Collaborative project*

Project acronym: SNM

Project full title: "**Single Nanometer Manufacturing for beyond CMOS devices**"

Grant agreement no: 318804

Deliverable: D7.5 ("Methodology for traceable characterization of probe-sample interaction and probe shape")

Name of the coordinating person: Prof. Dr. Ivo W. Rangelow, Email: ivo.rangelow@tu-ilmenau.de

List of participants:

Participant no.	Participant organisation name	Part. short name	Activity Type	Country
1 (Co)	Technische Universität Ilmenau	**TUIL**	HER	Germany
2	EV Group E. Thallner GmbH	**EVG**	IND; End-user	Austria
3	IMEC	**IMEC**	RES	Belgium
4	Mikrosistemi Ltd	**µS**	SME; End-User	Bulgaria
5	Universität Bayreuth	**UBT**	HER	Germany
6	Technische Universiteit Delft	**TUD**	HER	Netherlands
7	Spanish National Research Council	**CSIC**	RES	Spain
8	IBM Research GmbH	**IBM**	IND; End-user	Switzerland
9	École polytechnique fédérale de Lausanne	**EPFL**	HER	Switzerland
10	SwissLitho AG	**SL**	SME; End-User	Switzerland
11	Oxford Instruments Nanotechnology Tools Ltd	**OINT**	IND; End-user	UK
12	Imperial College London	**IMPERIAL**	HER	UK
13	The Open University	**OU**	HER	UK
14	Oxford Scientific Consultants Ltd	**OSC**	SME	UK
15	VSL Dutch Metrology Institute	**VSL**	IND	Netherlands
16	University of Liverpool	**ULIV**	HER	UK

SNM
Work Package 7
Deliverable: D7.5 ("Methodology for traceable characterization of probe-sample interaction and probe shape")

Lead beneficiary number	15	**Nature**	R	**Dissemination level**	PU
Estimated Person-months	5.0				

Person-months by partner for the Deliverable										
	VSL									
	5.0									

Estimated Delivery Date	M38: 03/2016	**Delivery Date**	04/05/2016
Author	• Arthur van de Nes, Richard Koops		
Reviewed by:	• WP7 Leader: Marijn van Veghel • WPG3 Leader: Mike Cooke • Coordinator: Ivo W. Rangelow		

Criteria and Achieved Results	**Criteria**	**Achieved result**
	Develop methodology for traceable characterisation of probe-sample interaction.	• Generalised AFM probe model for probe characterisation developed. • Various probe calibration samples prepared. • AFM scan range calibrated using virtual reference standard. • Traceable probe calibration methodology developed.

		• Traceable AFM measurements demonstrated using calibrated probe.
Description of the Deliverable	## Introduction In this document, a methodology is presented for the traceable characterisation of an AFM probe using samples with isolated spherical particles of varying size. Using a characterised AFM probe, the probe-sample interaction can be predicted and corrected for. Along with the calibration of the AFM scan range, the probe-sample interaction generally forms the dominant contribution to the uncertainty of AFM measurements. In order to arrive at a traceably characterised methodology for predicting the probe-sample interaction, we derive a generalised AFM probe model, discuss the selection procedure of metrological AFM probes, treat the preparation procedure of the required samples with spherical particles, explain the calibration procedure of a commercial AFM with virtual reference standards, demonstrate the procedure of the probe calibration, and perform traceable AFM line-width measurements using the developed techniques. ## Generalised probe model A generalised AFM probe model was developed to approximate the typical AFM probe shape, assuming a spherical tip with a conical shaft. To derive the probe parameters, an AFM measurement with the probe is assumed of a sample with spherical particles. The basic principle of the algorithm is described in deliverable D7.3, where the width and height of the identified particles are used to approximate the probe width, and to check the applicability of the used model. The initial step after an AFM measurement has been taken consists of tilt, offset, and drift correction. Based on the information provided by the manufacturer, a choice is made to either use the generalised probe model to obtain the probe parameters, or fix particular properties and force a match with a spherical, conical or cylindrical probe instead. The routine results in an effective radius, and if applicable an angle or slope of the probe. A schematic representation of the mathematical model is given in Figure 1. Initially, the probe is assumed perpendicular to the measurement surface.	

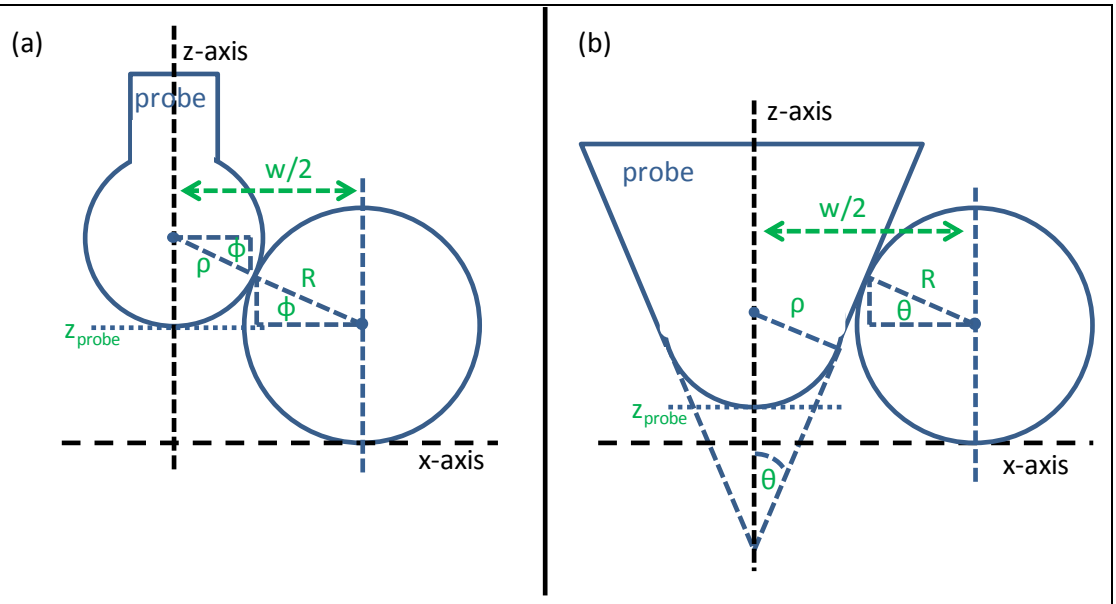

Figure 1 Generalised probe model, with ρ the effective probe radius, θ the probe angle parameter, *R* the spherical particle radius, and the measured particle width *w* at a specific probe height z_{probe}. For a maximum probe height equal to the particle diameter down to $z_{probe} = R - \rho$, the spherical model (a) is used, and further down to $z_{probe} = 0$, the conical probe (b) is used. Note that for a cylindrical probe the cone half angle θ is zero.

The measured width *w* of the spherical particle (including the effect of the probe) at a specific probe height z_{probe} can be expressed as

$$w = 2\left[4R\rho - z_{\text{probe}}^2 + 2z_{\text{probe}}(R-\rho)\right]^{1/2} \qquad \textbf{Eq. 1}$$

for a probe height ranging between

$$(R-\rho) + (R+\rho)\sin\theta \le z_{\text{probe}} \le 2R \qquad \textbf{Eq. 2}$$

And

$$w = \frac{2}{\cos\theta}\left[(R+\rho) + \left(R-\rho-z_{\text{probe}}\right)\sin\theta\right] \qquad \textbf{Eq. 3}$$

for a probe height ranging between

$$0 \le z_{\text{probe}} \le (R-\rho) + (R+\rho)\sin\theta \qquad \textbf{Eq. 4}$$

with *R* the spherical particle radius, ρ the effective probe radius, and *R* the probe angle. In case of a cylindrical probe cone angle θ is equal to zero.

The probe parameters are determined per identified spherical particle. Next, the ensemble of identified particles is considered, unusable particles removed (e.g. at the edge of the measurement region, in case of clusters, etc.), and the median probe

parameters are determined.

In case a distinct sub-regime can be identified corresponding with a fixed probe height, it is possible to use a simplification of the model above. For example, for a negligible probe height and a spherical or cylindrical probe, the measured width is equal to the particle diameter plus the probe diameter $w = 2(R + \rho)$. In case of a conical probe, negligible probe height and small probe angle, the measured width is equal to the probe diameter, the particle diameter, and a correction for the increasing conical width for the measured particle $w = 2(R + \rho) + 2(R - \rho)\theta$. With these relations, the probe parameters can be estimated. Using the variation in particle diameter of a sample of spherical particle distribution with a wide size distribution, a reduced standard deviation can be obtained of the estimated probe parameters.

The uncertainty of the determined probe parameters is difficult to estimate, but includes the standard deviation of the probe radius and cone angle. The fluctuations in these parameters originate partly from the measurement noise, but are also due to model assumptions, such as perfectly spherical particles, an accurate knowledge of the AFM scan position, meaning the position was calibrated for the used measurement range, and an idealized probe shape. In reality, any characterised probe parameter will merely be an approximation of the actual probe shape as decomposed to the mathematical model. In case one or more unrealistic probe shape values are found, such as a negative probe radius, the model assumptions have not been met.

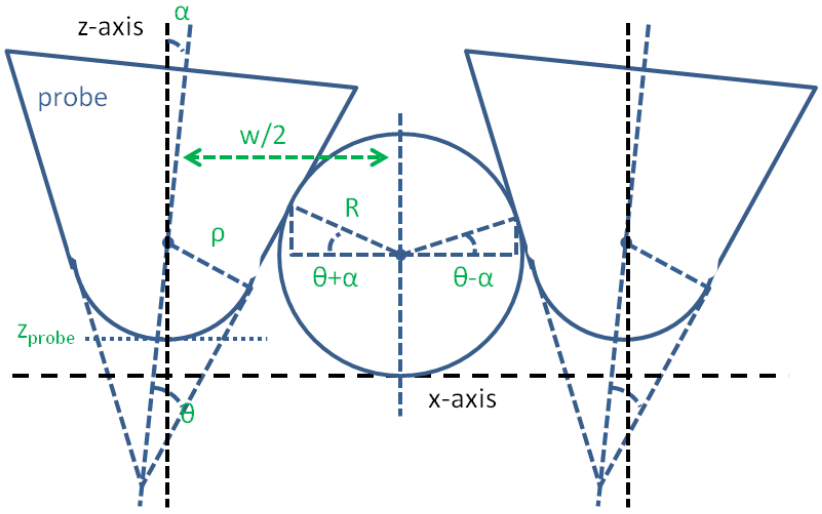

Figure 2 Generalised probe model for probe tilted by angle α.

In case the probe is tilted by angle α we can develop the model further, see Figure 2. Without loss of generality we assume the tilt angle positive, the measured width *w*

of the spherical particle including the effect of a probe tilted by, and at a specific probe height z_{probe} can be expressed as

$$w = 2\left[4R\rho - z_{\text{probe}}^2 + 2z_{\text{probe}}(R-\rho)\right]^{1/2} \quad \textbf{Eq. 5}$$

for a probe height ranging between

$$(R-\rho) + (R+\rho)\sin(\theta+\alpha) \leq z_{\text{probe}} \leq 2R \quad \textbf{Eq. 6}$$

The measured width is equal to

$$w = \frac{(R+\rho)\cos(\theta-\alpha) + \frac{1}{2}\left(R-\rho-z_{\text{probe}}\right)(\sin 2\theta + \sin 2\alpha)}{\cos^2\theta + \cos^2\alpha - 1} + \left[4R\rho - z_{\text{probe}}^2 + 2z_{\text{probe}}(R-\rho)\right]^{1/2} \quad \textbf{Eq. 7}$$

for a probe height, in case $\theta \geq \alpha$, ranging between

$$(R-\rho) + (R+\rho)\sin(\theta-\alpha) \leq z_{\text{probe}} \leq (R-\rho) + (R+\rho)\sin(\theta+\alpha) \quad \textbf{Eq. 8}$$

and for a probe height, in case $\alpha > \theta$, ranging between

$$(R-\rho) \leq z_{\text{probe}} \leq (R-\rho) + (R+\rho)\sin(\theta+\alpha) \quad \textbf{Eq. 9}$$

In case $\theta \geq \alpha$, the measured width is equal to

$$w = \frac{2\cos\theta}{\cos^2\theta + \cos^2\alpha - 1}\left[(R+\rho)\cos\alpha + \left(R-\rho-z_{\text{probe}}\right)\sin\theta\right] \quad \textbf{Eq. 10}$$

for a probe height ranging between

$$0 \leq z_{\text{probe}} \leq (R-\rho) + (R+\rho)\sin(\theta-\alpha) \quad \textbf{Eq. 11}$$

and, in case $\alpha > \theta$, the measured width is equal to

$$w = \frac{(R+\rho)\cos(\theta-\alpha) + \frac{1}{2}\left(R-\rho-z_{\text{probe}}\right)(\sin 2\theta + \sin 2\alpha)}{\cos^2\theta + \cos^2\alpha - 1} + (R+\rho) \quad \textbf{Eq. 12}$$

for a probe height ranging between

$$0 \leq z_{\text{probe}} \leq (R-\rho) \quad \textbf{Eq. 13}$$

Where the separation in regimes for a tilt angle larger or smaller than the cone angle is introduced as we expect the probe not to be able to probe underneath an object, schematically depicted in Figure 3. Note that the contribution of the probe tilt angle to the measured width for a cylindrical probe ($\theta = 0$) is approximately half that of the contribution of the probe angle of a conical probe, resulting in an ambiguity with

respect to the origin of measured probe parameter. This ambiguity can be resolved using a priori information about the probe, or by considering the two dimensional information available from the AFM measurements for the analysis.

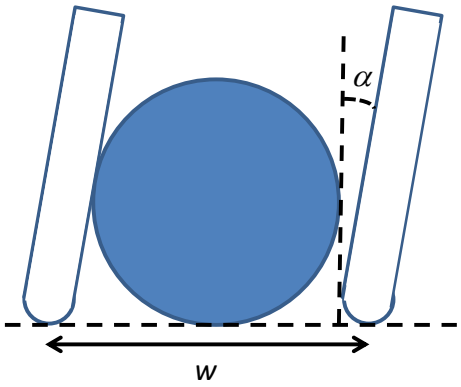

Figure 3 Schematic representation of the measured particle width and the probe tilt. Note the resemblance with half the cone angle as depicted in Figure 1b.

Selection of metrological AFM probes

The procedure to determine the metrological merits of AFM probes is discussed in deliverable D7.3 in detail. In general, the considered probe is initially characterised using the probe model, next it is intensively used during a series of measurements on a wear resistant sample lasting for several hours, and afterwards the probe is characterised again using the probe model, and finally the probe parameter before and after the probe wear measurements are compared. This way, two series of AFM probes were selected for their metrological merits and prove to be highly versatile for the commonly performed AFM measurements; the spherical probe B1_FMR and the carbon nanotube like probe CNT-100 or CNT-150 from nanotools, schematically represented in Table 1. Both probes are coated with diamond like carbon and show very little wear during the AFM measurements executed to stress the AFM probe. Whereas the spherical probe has a highly predictable probe-sample interaction, the nominal probe sphere radius of 20 nm is slightly too large for measurement of the smallest structures. Therefore the carbon nanotube like probe is better suited, having a nominal probe cylinder radius of 5 nm.

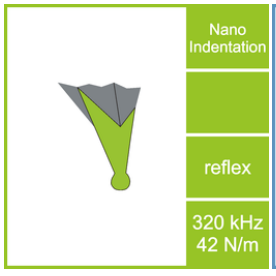

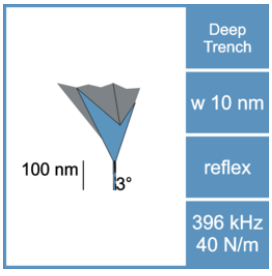

Probe type Tip	B1_FMR	CNT_100_ ArrowNCR	Probe type Cantilever	B1_FMR	CNT_100_ ArrowNCR
Material	HDC/DLC	HDC/DLC	Material	Si	Si
Shape	spherical	cylindrical	Shape	FMR	ArrowNCR
Tip length [nm]		100 (±20)	Length [µm]	225 (±10)	160 (±2)
Diameter [nm]		10 (±2)	Width [µm]	28(20-35)	45 (±1)
Half cone angle [°]		0	Thickness [µm]	3 (±1)	4.6 (±1.0)
Radius [nm]	20 (10-25)	<2 (<5)	Force const. [N/m]	2.8 (0.5-9.5	42 (35-45)
Tilt comp. [°]		3 (±0.5)	Reson. Freq. [kHz]	75 (45-115)	260 (±20)
Pyramid hght [µm]		15 (10-15)	Tip side	none	none
Tip set back [µm]		15 (5-25)	Back side	reflex	reflex

Table 1 Spherical (green) and carbon nanotube like (blue) AFM probes.

During the measurements presented in this document, we have used one spherical probe (B1_FMR, C2513169, probe 3), and three cylindrical probes (CNT-100, C2514027, probe 1; CNT-100, C2513166, probe 5; CNT-150, C2514241, probe 1) where the probe specific parameters as measured by the manufacturer are summarised in Table 2.

Serial number	C2513169	C2514027	C2514027	C2514027	C2514027	C2513166	C2514241
Probe number	3	1	2	3	4	5	1
Probe type	B1	CNT-100	CNT-100	CNT-100	CNT-100	CNT-100	CNT-150
Tip length [nm]		100 ± 20	97 ± 20	105 ± 20	99 ± 20	119 ± 20	179 ± 30
Diameter [nm]		10 ± 2	11 ± 2	10 ± 2	10 ± 2	10 ± 2	11 ± 2
Radius [nm]	19 ± 2						
Tilt comp. [°]		3	3	3	3	3	13
Shape	FMR	ArrowNCR	ArrowNCR	ArrowNCR	ArrowNCR	ArrowNCR	ArrowNCR

Table 2 Probe specific parameters for probes used for measurements presented in this document, as measured by the manufacturer.

Probe calibration sample preparation procedure

Several samples consisting of a mica substrate, a silicate mineral cleaved in order to obtain an ultraflat surface, with spherical particles deposited on it have been prepared to match with the anticipated probe shape and effective radius, and therefore allow for an accurate probe shape calibration. Multiple particle solutions were commercially obtained with different particle material and nominal radius. Both, samples with a narrow particle size distribution and with a wide particle size distribution were prepared. Samples with a wide particle distribution result in a lower uncertainty of the measured probe parameters, as a broader range of the parameter space can be used for the model fit reducing residual interdependency. The desired particle density on the substrate surface was obtained by optimising the dilution ratio of the particle solution before it was allowed to evaporate from the substrate. In some cases, the mica substrate was treated with poly-lysine to improve the bonding with the particles.

The samples used for the work presented in this document consist of larger particles with a nominal diameter of 60 nm and a wide size distribution, small gold particles with a nominal diameter of 5 nm and a wide size distribution, large silica particles with a nominal diameter of 50 nm and a narrow size distribution, and packed clusters of silica particles with a nominal diameter of 50 nm and a narrow size distribution, as shown in Figure 4.

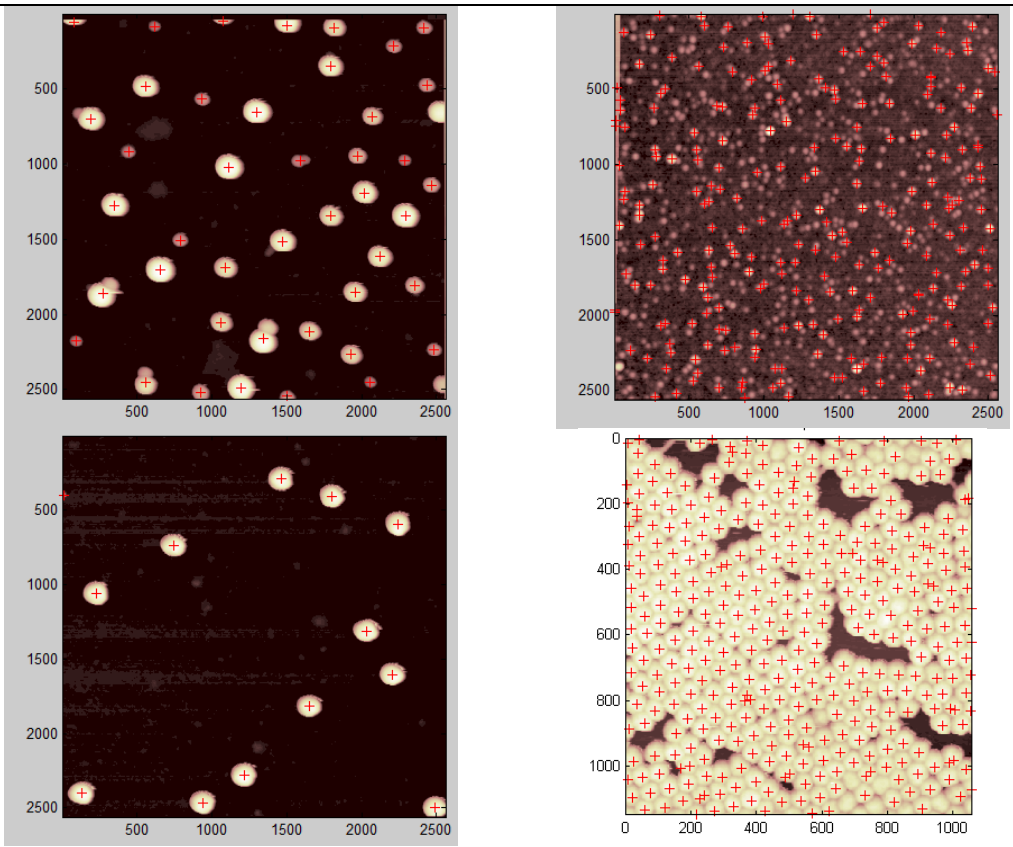

Figure 4 Large particles with a nominal diameter of 60 nm and a wide size distribution (left top), small gold particles with a nominal diameter of 5 nm and a wide size distribution (right top), large silica particles with a nominal diameter of 50 nm and a narrow size distribution (left bottom), and packed cluster of silica particles with a nominal diameter of 50 nm and a narrow size distribution (right bottom). The red cross hair indicates the centroid of a region indentified as particle.

AFM calibration procedure

In order to relate the AFM scan measurement results of the Veeco Dimension 3100 AFM to actual dimensions of the object under study, the required scan range of the AFM needs to be measured or calibrated. Examples of directly measured scan positions involve capacitive sensors or optical interferometers, requiring access to the scan stage. Calibration of the AFM scan range usually takes place using gratings with a well defined pitch for the lateral direction, and well defined step heights for the vertical direction, suffering from limitations in range and accuracy. In our case, the AFM scan range is calibrated using a virtual reference standard, see Figure 5. The virtual reference standard consists of two separately calibrated piezo transducers, one for the vertical scan range, and one for the horizontal scan range.

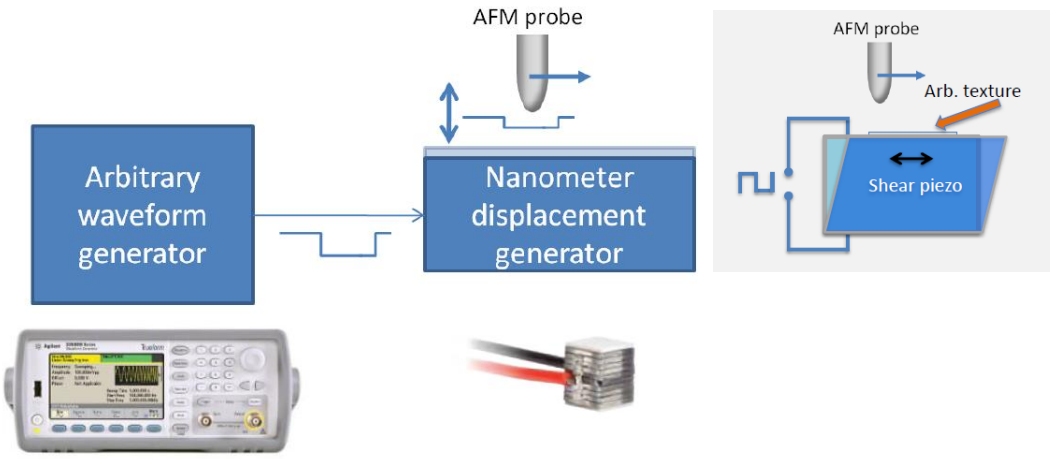

Figure 5 Virtual reference standard principle to calibrate the AFM.

For calibration of the vertical scan height, a calibrated piezo tranducer is modulated with a low frequency block function with fixed amplitude. From the AFM measurement the high and low regions are determined and the height can be calibrated.

For a calibration of the horizontal scan range, a calibrated shear piezo tranducer is modulated with a low frequency block function with fixed amplitude. From the AFM measurements, the two discrete surface profiles (shear piezo low, and shear piezo high) are determined, and the induced lateral change is obtained by correlating the images. Note, the non-linearity present in the AFM measurement is also corrected for using the calibration method.

The piezo tranducers were calibrated using an optical interferometer with an expanded uncertainty of 20 picometer (reference) over a large actuation range resulting in 1.978 nm/Vpp for the virtual height standard, and 2.167 nm/Vpp for the virtual lateral standard, when used with the corresponding waveform generator, where Vpp is the peak-to-peak amplitude of the waveform.

The calibration factors have been determined over a fixed scan range of 1.4 by 1.4 µm using the CNT-100 probe for both physical reference standards (see Figure 6) and the virtual reference standards (see Figure 7), resulting in the values presented in Table 3. In general, the values of virtual and physical reference standard match within one standard deviation. The standard deviation is determined over multiple AFM calibration exercises with varying AFM settings. Note that the standard deviation for the virtual reference standard is relatively large due to instabilities of unknown origin that the AFM experiences when using the CNT-100 probe. Based on

the technique the standard deviation should be an order of magnitude smaller. In case of a spherical B1-FMR probe, the standard deviation typically drops to a value of less than 0.005.

In general, the AFM calibration is repeated for each set of measurements in which the same scan range, AFM probe, and AFM settings are used.

	x	y	z	σ
virtual standard	0.95	0.97	0.94	0.01
physical standard	0.92	0.97	0.91	0.03

Table 3 Calibration factors and the standard deviation for a fixed scan range for multiple calibration efforts with varying AFM settings obtained with the virtual and physical reference standards.

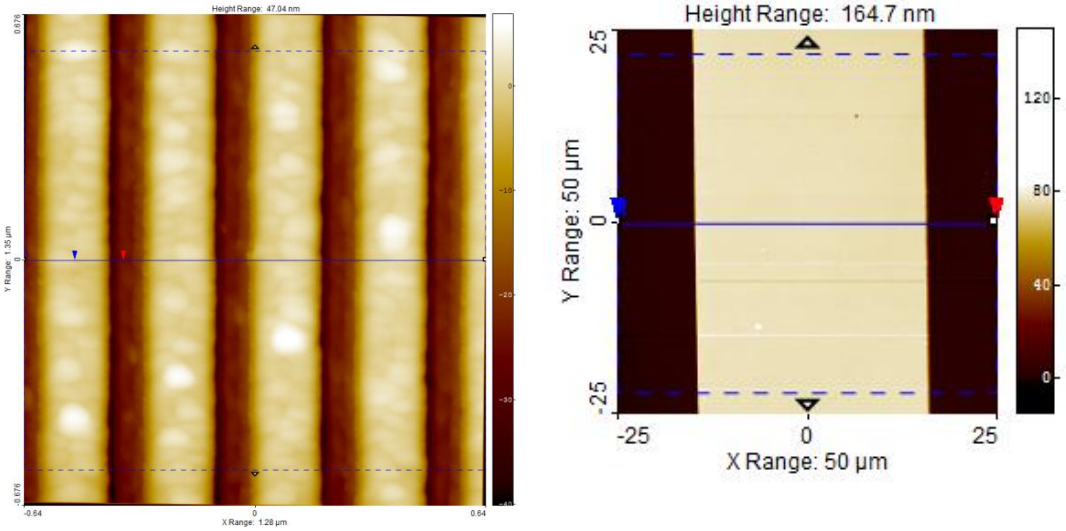

Figure 6 Physical reference standard calibration measurements. (Left) A grating with a pitch of 292 nm for the calibration of the lateral range. (Right) A height step of 68 nm for the calibration of the vertical range.

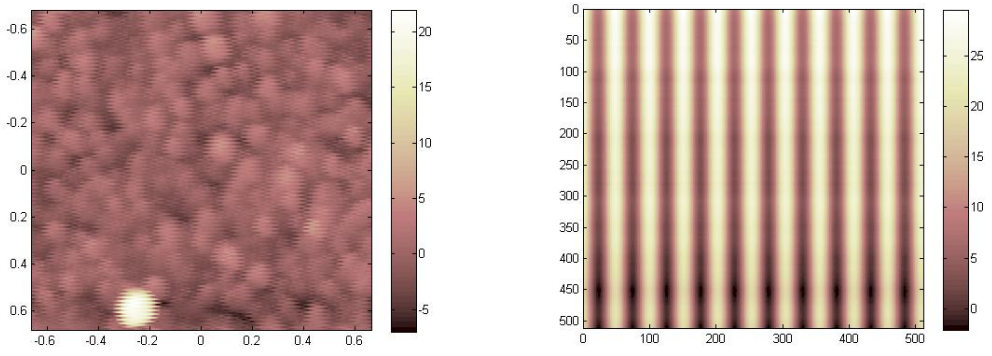

Figure 7 Virtual reference standard calibration measurements. (Left) Random surface topology, translated for every other line by 21.7 nm generated by a modulated piezo actuator, correlation of the deinterlaced image yields the calibration factor. (Right) Virtual step height of 19.8 nm generated by a modulated

piezo actuator yields the corresponding calibration factor.

Probe calibration

Using the sample with spherical particles with a nominal diameter of 60 nm and a wide size distribution, the spherical probe B1-FMR (C2513169, #3) has been calibrated using the probe model described previously. Two different approaches have been compared and are illustrated in Figure 8; the first approach fits the measured width of the identified particles versus the height of the AFM probe. The coefficients of the second order polynomial fit are related to the probe parameters, such as the sphere radius. The second approach uses the linear relation between measured height and measured width of the identified particles, where the slope should ideally be equal to 1, and the offset corresponds with the probe diameter. Deviations from the ideal slope of 1 of the measured width versus measured height curve could be due probe tilt, residual drift and non-linearities, or a mismatch in the probe model.

The probe radius as determined using the first approach is (23.5±0.9) nm, whereas the probe radius using the second approach is 19.2 nm in the x-direction and 18.4 in the y-direction. For the first approach, the standard deviation was determined taking into account only values within a band of 3σ of the median probe radius. For the second approach, an estimated standard deviation cannot easily be obtained for an individual measurement. For a series of repeated probe calibrations, the standard deviation is determined of the acquired probe radius for both the first and the second approach, as shown in Figure 9(left). The obtained radius and standard deviation for the probe as obtained using the width versus probe height is (23.1±0.4) nm, and when using the width versus particle height is (18.6±1.3) nm. The manufacturer specified the probe radius as (19±2) nm based on a SEM analysis. Although the second approach yields a value closer to the 19 nm as specified by the manufacturer, the first approach results in a smaller standard deviation and fits better when a series of measurements between the spherical and the cylindrical probes are compared, and will be discussed in the next section.

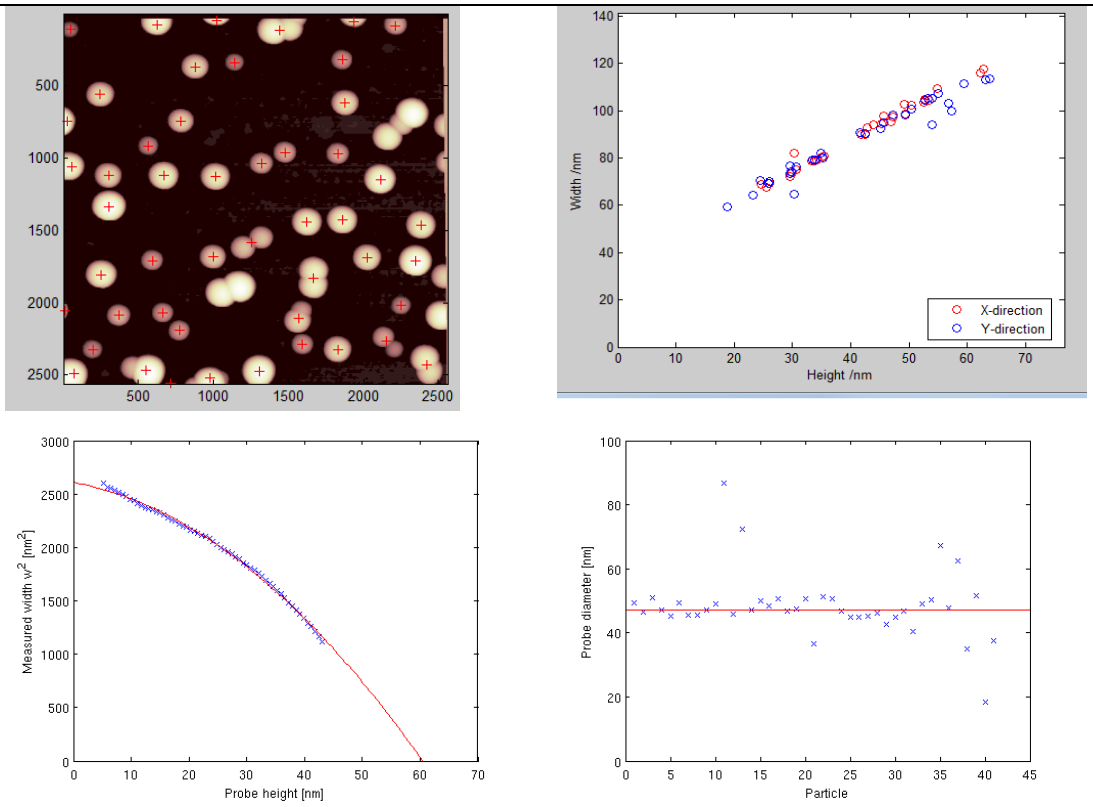

Figure 8 Particle sample measurement using a spherical probe (top left), measured width as a function of the particle height for the identified particles (top right), measured width as a function of probe height for an individual particle (bottom left), and retrieved probe diameter for all identified particles.

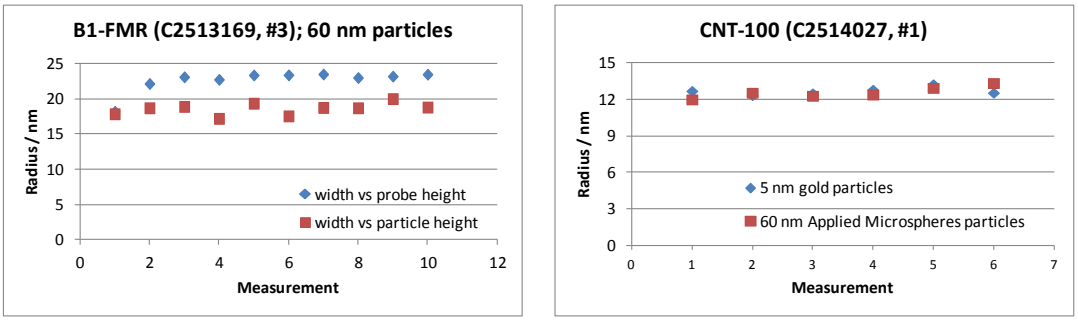

Figure 9 Repeated probe radius calibration derived as a function of the probe height (left) for a cylindrical CNT-100 probe, and derived as a function of the particle height (right) for a spherical B1-FMR probe.

Similarly, for the carbon nanotube like probe CNT-100 (C2514027, #1) the cylindrical probe radius has been determined, shown for the width versus probe height method in Figure 9(right). The probe radius was determined with the calibration samples with 60 nm particles and with 5 nm particles, resulting in (12.6±0.5) nm and (12.7±0.3) nm, respectively, demonstrating a good correspondence. A comparison with the alternative method yields (12.9±1.6) nm and (13.3±0.5) nm. Note that the probe radius is about twice the nominal value specified by the manufacturer

indicating wear, deformation or contamination of the probe. The probe has been returned to the manufacturer for confirmation of the increased probe diameter and contamination. The manufacturer measured the probe width using a SEM, resulting in a corrected probe radius of (9.5±2) nm, see Figure 10. The origin of the contamination could not be derived, but could be related to a residue of resist that was picked up by the probe.

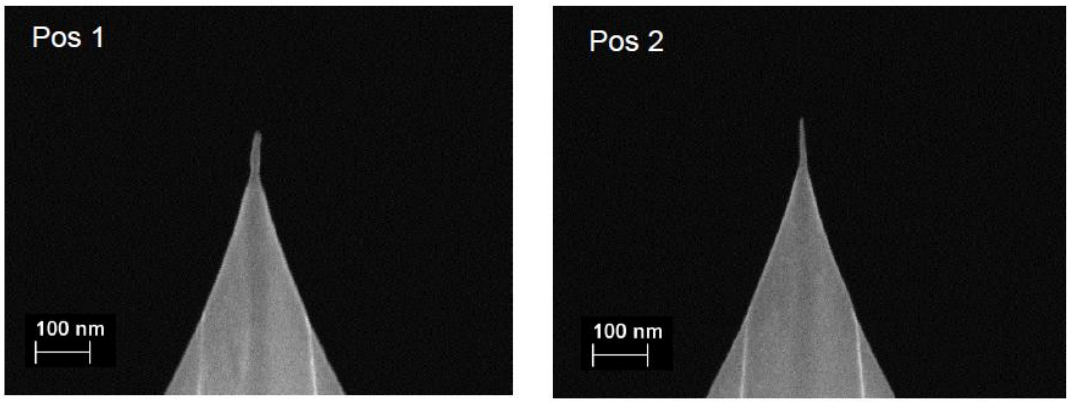

Figure 10 Recorded SEM image of two of the contaminated CNT-100 probes. The measured diameter of the structure is 19 nm (left), and 14 nm (right). Additionally, a reduction of the height of the probe tip was observed, yielding 80 nm (left), and 85 nm (right). The original specified diameter and height were 10 and 100 nm for probe #1 (left), and 11 and 97 nm for probe #2 (right), respectively.

Using the statistics presented above, it is possible to develop an uncertainty budget for the determination of the probe radius, summarised in Table 4. The dominant contribution is the numerical error due to the digital processing and modelling as collected in the standard deviation for the probe radius. Additional uncertainties are due to a potential deviation of the probe and particle shape from the used models. Randomly distributed deviations will average out, but systematic deviations, such as an asymmetry of the probe or particles, not. A possibly unnoticed residual asymmetry is estimated at a ratio of about 90% between the major and minor axis. In case the tilt of a probe is not taken in to account, this will also contribute to an error in the calibration of the probe radius. Additionally, the uncertainty in the calibration of the AFM scan range, estimated at a maximum of 1% for all axes, also affects the probe calibration. The combined expanded (k=2) uncertainty for the determination of the probe radius with the method outlined before, is for the spherical probe (B1-FMR) 5.0 nm, and for the cylindrical probe (CNT-100) 3.4 nm. An absolute measurement and uncertainty statement for the probe radius is essential for performing line-width measurements, but is not yet part of the documented dimensional measurements capabilities (see e.g. Bureau International des Poids et Mesures). Currently, a group of metrology institutes, including VSL, is performing a comparison of measurements on a specially designed line-width sample in order to

establish a reference uncertainty of line-width measurements (NANO6, organised by Euramet).

probe radius uncertainty estimate		B1-FMR	CNT-100
nominal probe radius		19	5
nominal particle radius		30	30
contributions		[nm]	[nm]
probe shape deviation			
lateral assymetry	0.9	1.0	0.3
vertical assymetry	0.9	1.0	0.3
particle shape deviation			
lateral assymetry	0.9	1.0	0.3
vertical assymetry	0.9	1.0	0.3
residual probe tilt			
uncompensated angle [deg]	10	0.0	0.4
numerical errors			
repeatability (std error)		1.5	1.5
AFM calibration	0.01	0.5	0.5
combined standard uncertainty		2.5	1.7
expanded standard uncertainty (k=2)		**5.0**	**3.4**

Table 4 Uncertainty estimate in the determination of the probe radius for the spherical probe (B1-FMR) and cylindrical probe (CNT-100).

Traceable AFM line-width measurements

For performing traceable line-width measurements using an AFM, the AFM was calibrated using the virtual reference standards, and the probe was characterised using the samples prepared with spherical particles, as discussed in the preceding sections. The line-width is determined from the SRAM-regions present on the IMEC sample as used for the internal benchmark of the measurement equipment used in the consortium, see Figure 11.

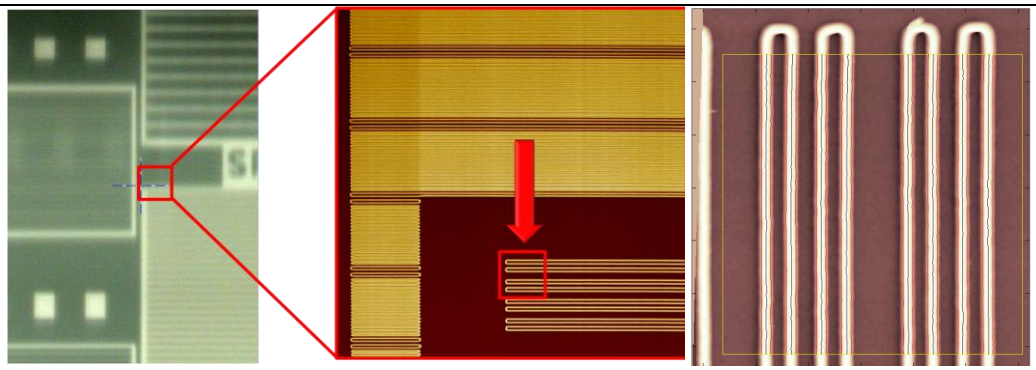

Figure 11 Location of the well separated lines on the IMEC sample, used for the traceable line-width measurements. The area in the yellow box (right), is the region used for the line-width measurements and measures about 1.3 by 1.3 µm.

To determine the uncertainty of the line-width measurements, multiple series were measured, each series of line-width measurements was followed by a measurement series of AFM probe characterisations, and vice versa. The line-width is measured as the full width at half the maximum height of the structure.

Initially, the AFM measurements series were executed using both the spherical probe B1-FMR and the cylindrical probe CNT-100 to determine the dependence on the AFM probe and confirm the validity of the developed models. The line-width is determined as the average over the 8 lines encountered. The raw line-width measurements for both probes can be corrected for a fictional probe radius and compared to check whether the corrected line-width regime overlaps, as shown in Figure 12.

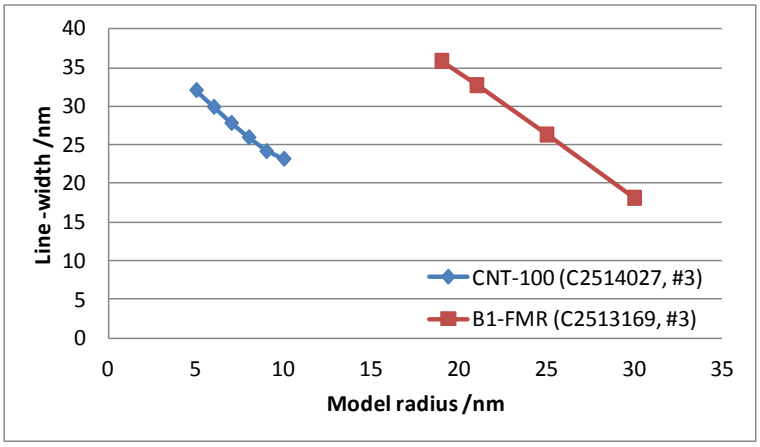

Figure 12 Measured line-width as corrected for a fictional probe radius with the spherical B1-FMR probe and the cylindrical CNT-100 probe.

The probe radius specified by the manufacturer for the spherical probe of 19 nm, would extrapolate to an unrealistically small probe radius of 3.3 nm for the cylindrical probe. The probe radius specified by the manufacturer for the cylindrical

probe of 5 nm, would interpolate to a realistic probe radius of 21.4 nm for the spherical probe. The previously determined probe radius of the spherical probe of 23.1 nm in the probe calibration section corresponds with a realistic cylindrical probe radius of 6.3 nm, and a corrected line-width of 29.4 nm. The cylindrical probe radius is determined as (7.9±0.4), (6.7±0.5) and (8.0±0.2) nm, for run 1, 2 and 3, respectively, using the width versus particle height method, see Figure 13. Note that the reported standard deviation is not the only contribution to the (expanded) uncertainty of the probe radius. The averaged line-width corresponding with the individual runs are (35.9±0.2), (38.4±0.4), and (42.1±0.6) nm, respectively, not yet corrected for the probe shape. The average probe shape corrected line-width is 25 nm with an expanded uncertainty of 5 nm.

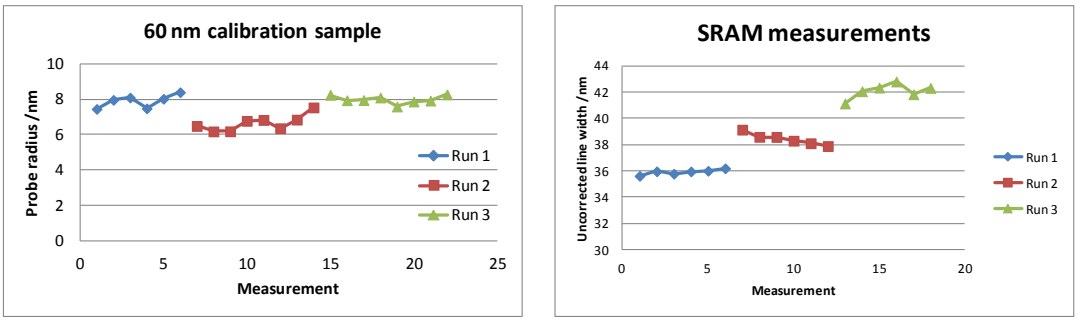

Figure 13 Characterised probe radius (left) and uncorrected line-width (right) for a total of 6 measurement series.

A second run has been performed with a slightly different cylindrical probe CNT-150 (C2514241, #1) with a tilt compensation angle of 13°, which is closer to the design value of 10° of the AFM. The characterised value for the probe radius for each measurement series is shown in Figure 14, resulting in (9.1±1.0), (7.6±0.7), (8.8±1.1), (7.7±1.1), and (9.5±0.6) nm, for the measurement runs respectively. The uncorrected line-width results in (43.5±1.8), (42.2±0.2), (40.2±0.8), (41.4±1.4), and (45.5±1.7) nm, for the measurement runs, respectively. The average probe shape corrected line-width is 25.5 nm with an expanded uncertainty of 5 nm.

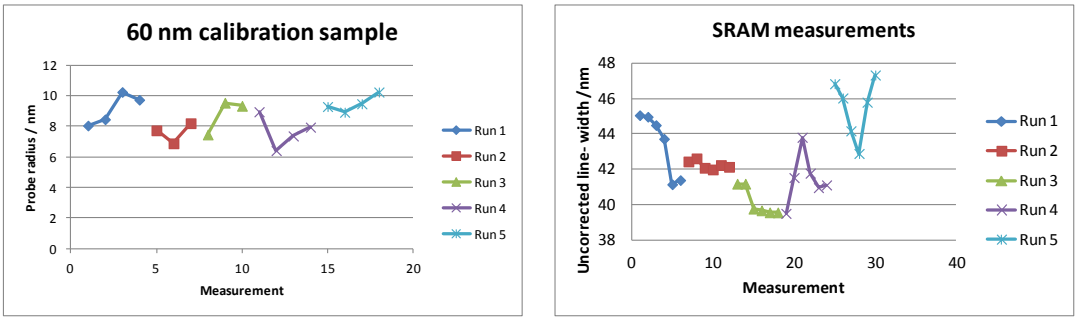

Figure 14 Characterised probe radius (left) and corrected line-width (right) for a total of 10 measurement series.

The uncertainty estimate for the AFM line-width measurements is summarised in Table 5. The uncertainty in the probe calibration forms the dominant contribution, but also the remaining absolute non-linearity error, the average error is zero, is relevant for the uncertainty estimate of the line-width measurement. Averaging in the slow-scan direction helps to increase the perceived resolution due to the choice of number of pixels and scan range. For larger structures, the relative error will become dominant in the error estimate, mainly dependent on the uncertainty associated with the scan range calibration.

AFM measurement uncertainty estimate				
scan range	1400	nm		
number of pixels/lines	512			
averaging length	100	nm		
contributions	[nm]		[L]	
averaged resolution	0.23			
calibration, 1% error for each axis			0.01	
Squareness error			0.0003	
Non-linearity residue	0.7			
Probe shape error	1.7			
combined standard uncertainty	1.9	nm	0.010	L
expanded standard uncertainty (k=2)	**3.7**	**nm**	**0.020**	**L**

Table 5 Uncertainty estimate for AFM measurements using probe calibrated using the presented methodology. The left column indicates the absolute contribution, and the right column indicates the relative contribution, which needs to be multiplied by the effective length *L* of the measured object.

Conclusion

A methodology has been developed for executing traceable AFM measurements. Therefore, the AFM probe is traceably characterised using a generalised AFM probe model in combination with samples with isolated spherical particles of varying size. Additionally, the AFM scan range is calibrated using a virtual reference standard. The measurement methodology results in an uncertainty estimate for the determination of the probe radius, and for the line-width AFM measurements.

Explanation of Differences between	The deliverable has been achieved.

Estimation and Realisation	
Metrology comments	The deliverable discusses the metrology aspects involved in order to perform AFM measurements corrected for traceable probe-sample interaction, please see the main text for more details.